1

Water Quantification of Amorphous and Crystalline Ferric Sulfates Relevant to Mars

Fan Meng[1#], Erbin Shi[1#], Changqing Liu[1], Zongcheng Ling[1]*

[1]Shandong Key Laboratory of Optical Astronomy and Solar-Terrestrial Environment, School of Space Science and Physics, Institute of Space Sciences, Shandong University, Weihai, Shandong, 264209, China.

Corresponding author: Zongcheng Ling (zcling@sdu.edu.cn)

Fan Meng and Erbin Shi contributed equally to this work.

Key Points:

- Seven amorphous ferric sulfates with specific hydration degrees (6w-12w) were synthesized.

- Water quantification of amorphous and crystalline ferric sulfates is achieved by Raman and LIBS spectroscopic methods.

- A new pathway of amorphous ferric sulfates by unsaturated solution is suggested to occur on Mars.

18   **Abstract**

19   Crystalline ferric sulfates (e.g., ferricopiapite and Fe(OH)SO$_4$) have been proposed at multiple
20   locations on Mars by the orbiter. While at Meridiani Planum and Gale Crater by rover missions,
21   amorphous ferric sulfates were also suggested to exist in soils and sedimentary rocks. The ferric
22   sulfates with different hydration degrees may play a key role in the water cycle on Mars. In order
23   to understand in detail the role of the hydrated ferric sulfates in the water cycle and their exact
24   hydration states on Mars, twelve ferric sulfates with different hydration states containing five
25   crystalline ferric sulfates and seven amorphous ferric sulfates were synthesized in the laboratory.
26   The water content (number of H$_2$O molecules) was quantified by Raman spectroscopy and
27   Laser-induced breakdown spectroscopy (LIBS), respectively. It was found that the amorphous
28   ferric sulfates water content has a good relationship with the SO$_4$ tetrahedron main Raman
29   feature position around 1000 cm^{-1}, the intensity and area of water feature around 3500 cm^{-1} over
30   SO$_4$ tetrahedron main Raman feature around 1000 cm^{-1}, respectively. Twelve ferric sulfates' Hα
31   emission line area at 656.7 nm is normalized by the O emission line area at 778 nm in LIBS
32   spectra. The crystalline and amorphous ferric sulfates all showed a good relationship between the
33   values of normalized results and the water content. These results will aid us in precisely
34   constraining the exact phases of hydrated ferric sulfates, provide a better reference for
35   ChemCam, SuperCam, and SHERLOC data interpretation and their use to quantify the water
36   content in detected targets.

37   **Plain Language Summary**

38   Hydrated ferric sulfates have been proposed to occur on Mars at different sites (e.g., Meridiani
39   Planum and Gale Crater) during orbital and rover missions. The hydration states of crystalline or
40   amorphous ferric sulfates are greatly affected by environmental conditions, and the amorphous
41   ferric sulfates are metastable phases, which are considered to be produced by rapid dehydration
42   and rehydration process. The presence of ferric sulfates indicates the occurrence of water-related
43   processes, while the water content within these compounds can provide valuable insights into
44   Mars' water history. However, the exact phases of ferric sulfates can not be precisely constrained
45   except for the jarosite that limited our knowledge about the water-related geochemical process
46   on Mars. In the present study, twelve hydrated ferric sulfates were synthesized in the laboratory
47   and measured by Raman and LIBS spectroscopy. The unique Raman features of those ferric
48   sulfates will help identify them on Mars by Raman spectroscopy. Besides, the methods of water
49   content quantification were developed based on their Raman and LIBS spectra, respectively. It
50   will help us to better understand the water cycle and provide a better reference for payloads like
51   ChemCam, SuperCam, and SHERLOC to determine the ferric sulfates on Mars.

52   **1 Introduction**

53   Ferric sulfates were inferred on Mars in the 1970s by the Viking Lander X-ray
54   fluorescence spectroscopic (XRFS) experiments (Toulmin et al., 1976). Based on the chemistry
55   results of Viking, Burns first proposed the existence of ferric sulfates on Mars in 1987 (Burns,
56   1987) including the jarosite and copiapite. These ferric sulfates were recognized as formed and
57   kept at low temperatures and pH conditions in Martian permafrost (Burns, 1987). The Mössbauer
58   spectra (MB) measured from Mars Exploration Rover (MER) Opportunity in the outcrops at
59   Meridiani Planum confirmed the presence of jarosite on the surface of Mars in 2004 (Madden et
60   al., 2004). Up to now, several ferric sulfates have been identified or suggested on Mars, such as
61   ferricopiapite, hydronium jarosite, and Fe(OH)SO$_4$ (Johnson et al., 2007; Lane et al., 2008;

62 Lichtenberg et al., 2010). These phases/minerals are products of evaporation and diagenetic
63 process. The ferric sulfates can not only provide mineralogical evidence clues for past water
64 activity on Mars but also hold a significant amount of water or hydrogen and play a key role in
65 the water cycle on Mars. Moreover, the hydration states of the ferric sulfates are very easily
66 changed due to minor variations in climate parameters, such as air, humidity, temperature, and
67 pH. Thus, ferric sulfates may be used to trace paleoclimate on Mars (Wang and Ling, 2011;
68 Wang et al., 2012). However, until now, the precision phases or hydration states of crystalline
69 ferric sulfates are still a big challenge. This is because the payloads on orbits and on rovers or
70 landers had a low resolution or can not use to exactly constrain the phases of targets and the
71 ferric sulfates occurred as various hydration states.

72   Except for the crystalline sulfates minerals identified at multiple locations on Mars, the
73 amorphous sulfates were also detected widely on the whole Mars surface and found that the
74 amorphous phases are a major component of Martian soils. The major compositions of
75 amorphous phases are clays and sulfates. At some local sites, the amorphous phases contain a
76 large percentage of SO_3, such as at Gale Crate and Meridiani Planum, which means sulfates or
77 sulfites may exist in amorphous phases (Glotch et al., 2006; Golden et al., 2005; Morris et al.,
78 2013). The high abundances (∼15-75 wt %) of X-ray amorphous components were identified
79 ubiquitously in ancient sedimentary rocks and soils in Gale Crater by the CheMin (XRD, CoKα)
80 on the Mars Science Laboratory rover Curiosity (Bish et al., 2013; Blake et al., 2012, 2013;
81 Treiman et al., 2016). In these X-ray amorphous phases in Gale Crater, the bulk SO_3 was found
82 to be about ∼20-90 wt % and the X-ray amorphous sulfur-bearing phase compositions are
83 consistent with mixtures of Mg-S, Fe-S, and possibly Ca-S phases, likely sulfates or sulfites
84 (Smith et al., 2022). Furthermore, ChemCam's laser-induced breakdown spectroscopy on the
85 Curiosity suggests that the amorphous materials in Gale Crater also contain a significant amount
86 of hydrogen, such as the Rocknest aeolian deposit containing 5-9 wt % hydrogen (Meslin et al.,
87 2013). As mentioned above, it has been demonstrated that ferric sulfates are not only present in
88 amorphous materials but may also have a certain degree of hydration. Various proportions, or
89 various degrees of hydration of this amorphous phase like ferric sulfates in the soil or
90 sedimentary rocks, could be sufficient to explain the global hydrogen variations seen from the
91 orbit by Gamma Ray spectrometer on Odyssey (Feldman et al., 2002).

92   Phase transitions and stability of the sulfate phase at Mars-related temperatures and
93 pressures have been widely investigated (Ling and Wang, 2010; Wang and Ling, 2011; Wang et
94 al., 2012; Wang et al., 2013; Wang and Zhou, 2014). These studies suggest that amorphous ferric
95 sulfate on the surface of Mars can persist under Martian conditions. RH fluctuations on the
96 surface of Mars will change the water content of the amorphous ferric sulfate but will not result
97 in crystallization. Amorphous ferric sulfate has previously been shown to dehydrate rapidly
98 through saturated solutions (Wang et al., 2012; Xu et al., 2009). Wang et al. (2020) showed that
99 electrostatic discharge would trigger an electrochemical reaction that would alter the material on
100 the surface of Mars, making it amorphous. Repeated slope linearization suggests that there is
101 currently an active brine cycle on Mars, which could facilitate the formation of amorphous
102 sulfates on the Martian surface (Bishop et al., 2021; Chevrier and Altheide, 2008; McEwen et al.,
103 2011). It is important to determine the specific hydration degrees of ferric sulfate relative to the
104 Martian surface environment and atmospheric environment. Crystalline and amorphous ferric
105 sulfates have been characterized by spectroscopic methods in some previous works (Cloutis et
106 al., 2006; Dyar et al., 2013; Sklute et al., 2015; Sklute et al., 2018; Wang et al., 2012). However,
107 to date, only a few studies have explored if there are any trends with amorphous sulfates and

108 abundance, or explored if there is systematic variation between crystalline or amorphous ferric
109 sulfates and their hydrogen content on Mars (Sobron et al., 2012).

110 Although significant amounts of sulfates have been found on the Martian surface, more
111 experimental data are needed to confirm which sulfates are present and to extract information
112 about historical hydration levels and the possibility of supporting life on Mars (King et al., 2010;
113 Lane et al., 2008; Sobron et al., 2012). Raman spectroscopy, which can provide detailed
114 information about chemical structures, phases and polymorphs, crystallinity and molecular
115 interactions, is an ideal tool for microscopic sample analysis of rock samples collected from the
116 surface of Mars (Chou et al., 2013; Vandenabeele et al., 2014; Wang et al., 2015). Raman spectra
117 contain a series of features corresponding to different vibrational modes in molecules. The
118 positions and line widths of these peaks are so unique to a system that they are considered to be
119 the "fingerprints" of molecular species. Therefore, Raman spectrometers are also being selected
120 as payloads for Mars exploration. The Perseverance rover landed in Jezero Crater in February
121 2021, carrying several scientific instruments, two of which are Scanning Habitable Environments
122 with Raman and Luminescence for Organics and Chemicals (SHERLOC) and SuperCam
123 (Bhartia et al., 2021; Lopez-Reyes et al., 2023; Moeller et al., 2021; Phua et al., 2023, Wiens et
124 al., 2021). The SHERLOC and SuperCam are the first two Raman spectrometers to be ever
125 employed in planetary exploration missions. Different secondary minerals have been identified
126 by the SHERLOC including carbonates, phyllosilicates, perchlorates, sulfates, and amorphous
127 (Hurowitz et al., 2023; Lopez-Reyes et al., 2023; Phua et al., 2023). Among the sulfates, the Ca-
128 and Mg- sulfates with different hydration states, such as the polyhydrated Mg-sulfates and
129 anhydrite Ca- sulfates, were suggested. However, characterizing hydration in these minerals is
130 not easy in some detected targets by the total area of OH band as a function of sulfate v_1 peak
131 position and intensity, respectively (Phua et al., 2023). Hence, new methods should be developed
132 to characterize hydration degrees for those secondary minerals.

133 LIBS is a rapid, portable, in situ atomic spectroscopy technique used to measure the
134 concentration of major and trace elements in solid, liquid, or air samples, or to record the
135 chemical signature of a material (Harmon et al., 2013; Pathak et al., 2012). LIBS is a spot
136 analysis technique, it is possible to evaluate spatial changes in material composition and also to
137 average shots taken from many different locations on the materials to obtain a bulk composition
138 (Jin et al., 2022; Liu et al., 2022; Meslin et al., 2013). As a powerful spectroscopic technology
139 for chemical composition analysis, LIBS helps to extract the elemental information of the rocks,
140 minerals, and soil of Mars (Jin et al., 2022; Liu et al., 2022; Meslin et al., 2013; Schröder et al.,
141 2015). LIBS technology has been deployed on Mars aboard different rovers since 2012,
142 including ChemCam on Mars Science Laboratory Rover Curiosity, MarSCoDe on Tianwen-1
143 Rover Zhurong, and SuperCam on Mars 2020 Rover Perseverance (Liu et al., 2022; Jin et al.,
144 2022; Wiens et al., 2012; Wiens et al., 2021). Based on the measured results of LIBS on Mars,
145 the major, minor, and trace elements were quantified using emission intensities of the respective
146 elements, including Fe, Mg, Ca, Li, Rb, Sr, Ba, etc. However, the quantification of nonmetallic
147 elements is challenging due to the numerous facts which influence the LIBS signal. Such as the
148 quantification of hydrogen by the Balmer alpha emission peak (656.6 nm). The peak at 656.6 nm
149 is much wider and the part overlapped with the C signal (Rapin 2019, 2016). Moreover, the
150 strongest signal position of some nonmetallic elements' is out of the LIBS measured range.
151 Therefore, it is necessary to develop a new method or optimize parameters to quantify
152 nonmetallic elements in different materials, especially the hydrogen content in different materials
153 on Mars, which will be significant for subsequent geological interpretations and has broad

154 implications for habitability studies. Rapin et al. (2016, 2019) and Nachon et al (2014)
155 constrained the water content of the calcium sulfate veins targeted on Mars by LIBS. It is
156 important to understand the information about past aqueous activity on Mars in terms of
157 temperature, humidity, and salinity (Nachon et al., 2014; Rapin et al., 2016, 2019).

158 The goals of this study is to synthesize different hydrated amorphous and crystalline
159 ferric sulfates in the laboratory, to fulfill precisely determined hydration states of different ferric
160 sulfates by combining Raman and LIBS technologies. Develop LIBS and Raman methods to
161 quantify the water content of amorphous and crystalline ferric sulfates to help evaluate the water
162 content in soils and rocks, and help to understand the aqueous history and environmental
163 evolution. The exact identification of these ferric sulfates and quantification of their hydrogen
164 content are important for understanding the soil or rock compositions and environmental
165 conditions that produced hydrated phases, water cycle on Mars.

166 **2 Experiments and Instruments**

167 2.1 Synthesis of twelve kinds of ferric sulfates

168 For the synthesis of seven amorphous ferric sulfates with different hydration degrees. The
169 ferric sulfate powder was first dissolved in deionized water to obtain a solution of ferric sulfate.
170 Its concentrations were fixed at 28.6 wt % and 5 wt %, respectively. Then these solutions were
171 put into seven PTFE Petri dishes, respectively, and the mass of the solutions in each petri dish is
172 4 g or 5 g (Table 1). After that, the seven Petri dishes which contain the solutions were put into
173 saturated LiBr buffer (relative humidity, RH% = 5.23%) solutions under 70°C for different hours
174 (12 h - 48 h). The synthesized seven kinds of amorphous ferric sulfates occurred as transparent
175 glass and with the increase of water content the color of them from light yellow to reddish
176 (Figure 1).

177 **Table 1.** Synthesis conditions of amorphous ferric sulfate with different hydration degrees.

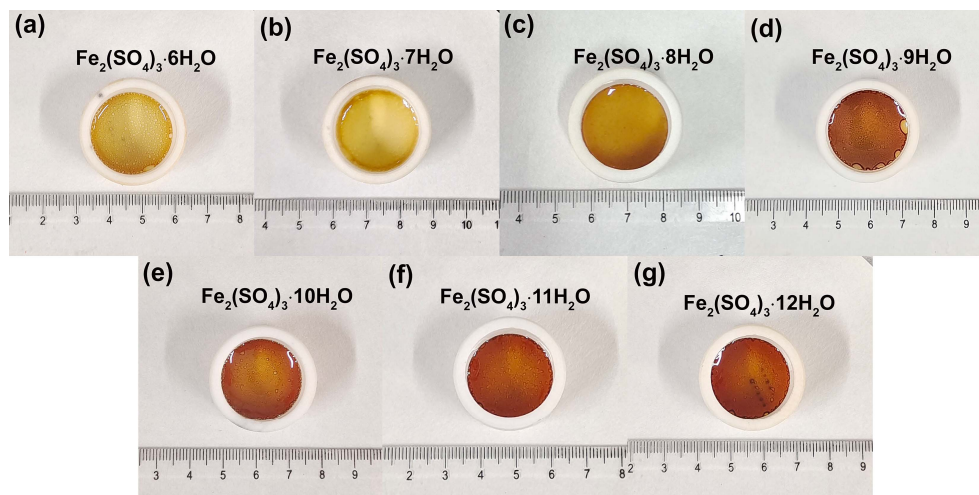| Sample	Temperature	RH% buffer	Concentration	mass	Time
$Fe_2(SO_4)_3 \cdot 12H_2O$	70 °C	LiBr	28.6 wt %	4 g	~12 h
$Fe_2(SO_4)_3 \cdot 11H_2O$	70 °C	LiBr	28.6 wt %	4 g	~15 h
$Fe_2(SO_4)_3 \cdot 10H_2O$	70 °C	LiBr	28.6 wt %	4 g	~18 h
$Fe_2(SO_4)_3 \cdot 9H_2O$	70 °C	LiBr	28.6 wt %	4 g	~24 h
$Fe_2(SO_4)_3 \cdot 8H_2O$	70 °C	LiBr	28.6 wt %	4 g	~48 h
$Fe_2(SO_4)_3 \cdot 7H_2O$	70 °C	LiBr	5.0 wt %	5 g	~24 h
$Fe_2(SO_4)_3 \cdot 6H_2O$	70 °C	LiBr	5.0 wt %	5 g	~48 h

178

179

Figure 1. Optical image of seven amorphous ferric sulfates. With the H_2O molecules increased the color of the samples from light yellow to reddish.

The five crystalline ferric sulfates with different hydration states were synthesized first in the laboratory. The rhomboclase was synthesized by the 10 mL saturated ferric sulfates solution added 0.6 g concentrated sulfuric acid at 50°C for 1 day. The pentahydrate ferric sulfate was prepared used the hydrothermal method. The 1.52 mL deionized water and 0.48 mL concentrated sulfuric acid using to solve the 1.98 g ferric sulfates powder. Then the solution was transferred to an autoclave at 90 °C for one week. The kornelite was synthesized using $Fe_2(SO_4)_3 \cdot xH_2O$ powder (Sinopharm Chemical Reagent Co. LTD, CAS:142906-29-4, $\geq$ 99%, Shanghai) under 95°C in $KI-H_2O$ saturated solutions (RH% = 59.92%) for 24 h in an oven (Ling and Wang, 2010). The paracoquimbite was synthesized at 25°C in $NaBr-H_2O$ saturated solutions (RH% = 57.58%) using the synthesized ferricopiapite as the starting material for three weeks. The ferricopiapite was synthesized using the ferric iron sulfate saturated solution at 25°C and the RH% ranged from 20% to 60% in the atmosphere for one week until the liquid solutions were entirely converted to solid. The $Fe(OH)SO_4$ was synthesized by heating the melanterite for three days at 180°C.

The phase identification of twelve synthesized samples was made by laser Raman spectroscopy and the seven amorphous ferric sulfates were then employed by XRD (Figure 2). For five crystalline samples, Raman data of more than 100 points were collected from a flattened powder sample that is placed on a glass slide, to confirm its homogeneity (Figure 3a). Seven amorphous ferric sulfates were characterized in Petri dishes directly (Figure 3b). The 2 theta of XRD were run in the 5-70° range with an increment of 0.02°and 5° per minute (Figure 2).

2.2 Instruments

An inVia® Raman imaging system (Renishaw Company) was used, which uses a 532-nm line of a DPSS laser for excitation, and a long-working-distance 50 × objective (NA = 0.75) for signal collection. The Raman spectra from 100 to 1400 cm^{-1} were collected for five crystalline ferric sulfates and from 100 - 4000 cm^{-1} for seven amorphous ferric sulfates (Figure 3). The inVia system has a spectral resolution better than 1 cm^{-1} and spectral repeatability of $\pm$ 0.2 cm^{-1}. The spectral wavelength was initially calibrated using the emission lines of the Ne lamp. The Raman peak position of a Si wafer (520.7 cm^{-1}) was checked and corrected on inVia at the

211 beginning and the end of every working day. These two calibrations ensure a Raman peak
212 position accuracy of $\pm$ 0.2 cm^{-1} in this study.

213   Laser-induced breakdown spectroscopy (LIBS) initiated by laser ablation of the samples
214 in a vacuum chamber (Liu et al., 2021; Wu et al., 2021) with the simulated atmospheric
215 environment of Mars (CO_2, ~7 mbar) and Earth environment, respectively, at Shandong
216 University, Weihai. The system has been equipped with a Q-switched pulsed Nd: YAG laser
217 with a power of 200 mJ and a wavelength of 1064 nm. The corresponding laser fluence was
218 about 83.56 J/cm^2, and the average diameter of the laser-focused spot size on the sample was 400
219 μm. The synthesized ferric sulfate samples were pressed under a pressure of ~20 MPa for 90 s to
220 form a pellet with a diameter of 4 cm. The synthesized amorphous ferric sulfate samples were
221 directly measured in the dishes. Six spectra were collected at different locations for each sample
222 with different laser energy used. After obtaining the LIBS spectra, the noise and continuous
223 background were removed using the wavelet function and spline function (Liu et al., 2021),
224 respectively. Six spectra were collected for every sample and every spectroscopy of them is
225 acquired by an accumulation of ten shots.

3 Results

3.1 Phases identified of twelve ferric sulfates

228   The hydration degrees of seven amorphous ferric sulfates were determined by mass-
229 change measurements. The starting materials ($Fe_2(SO_4)_3 \cdot xH_2O$ powder, Sinopharm Chemical
230 Reagent Co. LTD, CAS:142906-29-4, $\geq$ 99%, Shanghai) were heated to 220 °C in a muffle
231 furnace for 3 days to make it completely converted to mikasaite ($Fe_2(SO_4)_3$). The water content
232 of different amorphous was calculated by the mass loss of the ferric sulfates solution after being
233 completely converted to solids. Finally, the number of H_2O molecules for per $Fe_2(SO_4)_3$ were
234 derived from $Fe_2(SO_4)_3 \cdot 6H_2O$ to $Fe_2(SO_4)_3 \cdot 12H_2O$. Moreover, the stability of the seven
235 amorphous ferric sulfates was studied. We found that the synthesized seven amorphous ferric
236 sulfates could be kept for at least 24 hours when sealed by parafilm in Petri dishes. Thus, all
237 measurements in the study were performed within one day to make sure all results are convinced.
238 The hydration states of five crystalline ferric sulfates were determined by their standard Raman
239 spectra published by Ling and Wang in 2010 (Ling and Wang, 2010).

3.2 The Raman spectra of synthesized ferric sulfates

241   All measured Raman spectra of five crystalline ferric sulfates and seven amorphous ferric
242 sulfates are identical to the standard Raman spectra and no other phases were detected, which
243 indicated that the samples are homogeneous. The wavenumber range was 100 - 4000 cm^{-1}, which
244 was divided into three regions according to the origin of characteristic peaks. The Raman peaks
245 in the first region (150 - 1500 cm^{-1}) can be attributed to the different vibration modes of the SO_4
246 tetrahedron. Among them, the features in the range of 930 - 1100 cm^{-1} are attributed to the
247 symmetric stretching (v_1) vibration of SO_4 tetrahedra, the features in the range of 350 - 550 cm^{-1}
248 are attributed to the symmetric bending (v_2) vibration of SO_4 tetrahedra, the features in the range
249 of 1100 - 1200 cm^{-1} can be assigned to the asymmetric stretching (v_3) vibration of SO_4
250 tetrahedra, and the features in the range 550 - 700 cm^{-1} are attributed to the asymmetric bending
251 (v_4) vibration of the SO_4 tetrahedra (Ling and Wang, 2010; Nakamoto, 1978). The characteristic
252 peaks in the range of 1600-1800 cm^{-1} can be attributed to the bending vibration of H_2O. The

253   characteristic peaks in the range of 3000-3600 cm^{-1} can be attributed to the symmetric and
254   antisymmetric stretching vibration of H_2O. The detailed assignment of these Raman features can
255   be found in a paper published by Ling and Wang in 2010. For seven amorphous ferric sulfates
256   with different water contents, we found that all Raman peaks had large widths, indicating that the
257   synthesized samples are amorphous. This result was further confirmed by the XRD
258   measurements. All seven amorphous ferric sulfates XRD patterns show a broad peak around 25°
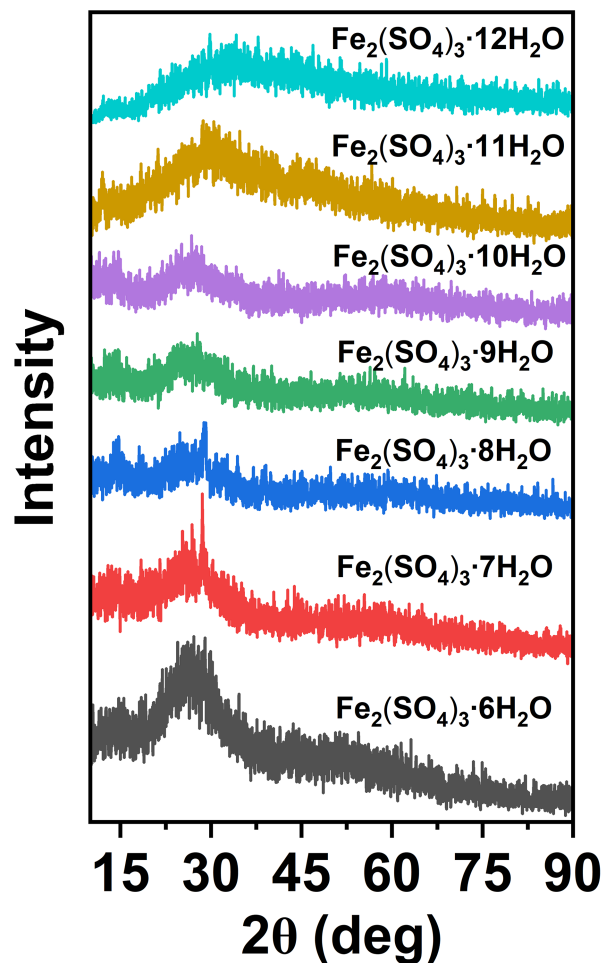259   which means the synthesized samples are amorphous phases (Figure 2).

260

Figure 2. XRD patterns of seven amorphous ferric sulfates. All of them showed a broad feature
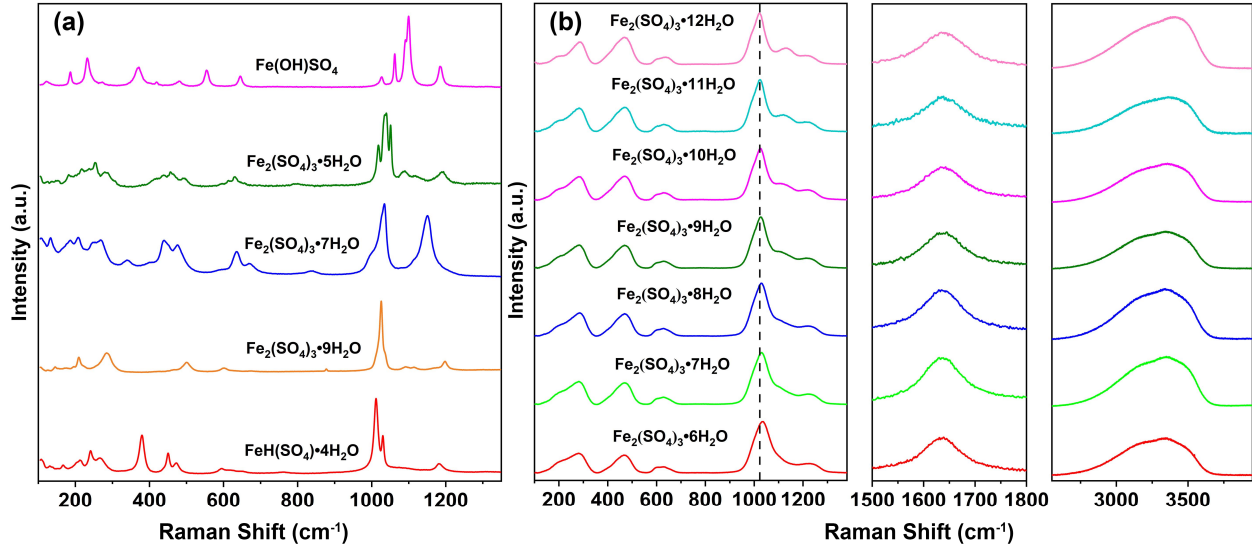262   around 25° demonstrating they are amorphous phases.

263

Figure 3. Raman spectra of twelve synthesized ferric sulfates. (a) Five crystalline ferric sulfates Raman spectra in the range 100 - 1400 cm^{-1}. (b) Seven amorphous ferric sulfates Raman spectra in the range 100 - 4000 cm^{-1}; For the seven amorphous ferric sulfates the main features around 1000 cm^{-1} shift to low wavenumber with increase the hydration degrees.

3.3 The Raman spectra of synthesized ferric sulfates

The Raman spectra of seven amorphous ferric sulfates were analyzed to find the relationship among the peak positions, peak intensities, peak areas, and the number of water molecules. The Gauss-Lorentz mixture function in WIRE 3.4 software was used to fitting the peaks around 1000 cm^{-1} and 3500 cm^{-1} and found that with the hydration degree increased the peak positions shift to the low wavenumber, and the hydration degrees of amorphous ferric sulfates had a linear relationship with the peak positions (Figure 4a). The linear fitting was carried out on it, and the fitting result was:

$$R_{1000} = -2.00 \ W + 1041.5, \ R^2 = 0.989$$

where R_{1000} is the Raman shift of SO_4 tetrahedron Raman peak around 1000 cm^{-1}, and W is the water content of the synthetic sample.

By fitting the peaks of water around 3500 cm^{-1} and SO_4 tetrahedron around 1000 cm^{-1}, the peak intensities and peak areas were obtained, respectively. It is found that the peak intensities and peak areas ratio of water features over SO_4 tetrahedron features are related to water content, respectively. With the increase of H_2O molecules, the ratios of peak intensities and peak areas of H_2O over SO_4 tetrahedron between 3500 cm^{-1} and 1000 cm^{-1} are increased. The linear fitting was also carried out on it, and both of them are shown a good linear relationship (Figure 4b and 4c). The relationship between peak intensities ratio versus the number of H_2O molecules in amorphous ferric sulfates is:

$$I_{3500/1000} = 0.0296 \ W + 0.0476, \ R^2 = 0.990$$

The relationship between peak areas ratio versus the number of H_2O molecules in amorphous ferric sulfates is:

$$A_{3500/1000} = 0.2183 \ W + 0.5813, \ R^2 = 0.995$$

292   where I is the intensity of Raman peaks, $I_{3500/1000}$ is the ratio of peak intensities of H_2O
293   over SO_4 tetrahedron between 3500 cm^{-1} and 1000 cm^{-1}, A is the area of Raman peaks, $A_{3500/1000}$
294   is the ratio of peak areas of H_2O over SO_4 tetrahedron between 3500 cm^{-1} and 1000 cm^{-1}, and W
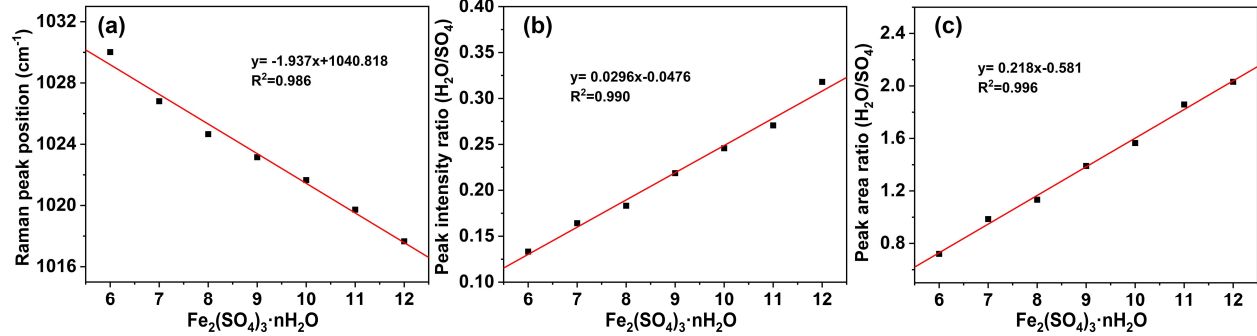295   is the water content of the synthetic sample.

297   **Figure 4**. The linear fitting of the number of H_2O molecules in seven amorphous ferric sulfates
298   with (a) peak positions, (b) peak intensities ratio of H_2O at 3500 cm^{-1} over SO_4 tetrahedron at
299   1000 cm^{-1}, and (c) peak areas ratio of H_2O at 3500 cm^{-1} over SO_4 tetrahedron at 1000 cm^{-1},
300   respectively; All of them are shown a good linear relationship.

301   3.4 LIBS spectra general analysis

302   The LIBS spectra of five crystalline ferric sulfates were measured under the Earth and
303   simulated Mars environment, respectively (Figure 5a and 5b). However, the seven amorphous
304   ferric sulfates were only measured under the Earth environment (Figure 6) because they change
305   easily under simulated Mars conditions. Furthermore, these amorphous ferric sulfates measured
306   voltage is different from crystalline ferric sulfates. The amorphous phases were measured at 750
307   V and the crystalline ferric sulfates were measured at 820 V. This is because the amorphous
308   LIBS signal reaches saturation at 820 V, while the signal intensity of crystalline ferric sulfate is
309   weaker at 750 V. Hence, the ferric sulfates were recognized as two systems. All LIBS spectra of
310   twelve ferric sulfates can be divided into three spectral regions. The Fe emission lines dominate
311   in the UV, Blue, and VIS-NIR spectral regions (Perkins et al., 2009). The hydrogen emission line
312   is produced from the dissociation of the water molecules and hydroxyl appears at 656.7 nm. The
313   oxygen lines around 778 nm can be attributed to oxygen in sulfate ions (SO_4^{2-}), water molecules,
314   and hydroxyl (OH^-) in ferric sulfates. However, no matter what is measured conditions of all
315   twelve ferric sulfates LIBS spectra are not produced S lines. This is because the detection limit
316   of the sulfur element is higher than other elements and the LIBS system's performance is not
317   good. Moreover, the LIBS spectra of the same crystalline ferric sulfates measured under Earth-
318   and Mars-like environments are different. In the UV region (238 - 400 nm), the intensity of LIBS
319   signal under the Earth environment is weaker than in Mars-like environments. Oppositely, in the
320   VIS-NIR region, the peak intensity of LIBS under the Earth's environment is higher under
321   simulated Mars conditions (Figure 5). Furthermore, the ratio of signal to noise is higher and the
322   peak width of iron and oxygen emission lines are narrow under a Mars-like environment. These
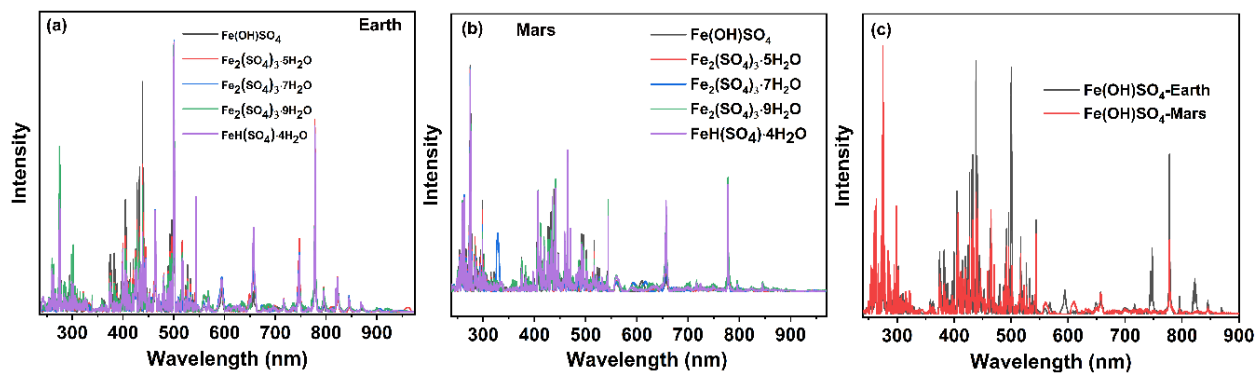323   results are due to the physical matrix effects.

Figure 5. The LIBS spectra of five ferric sulfates were obtained from (a) the Earth environment and (b) Mars-like conditions; (c) The LIBS spectra of Fe(OH)SO$_4$ were acquired from Earth and Mars conditions, respectively, to evaluate the effects of the environment.
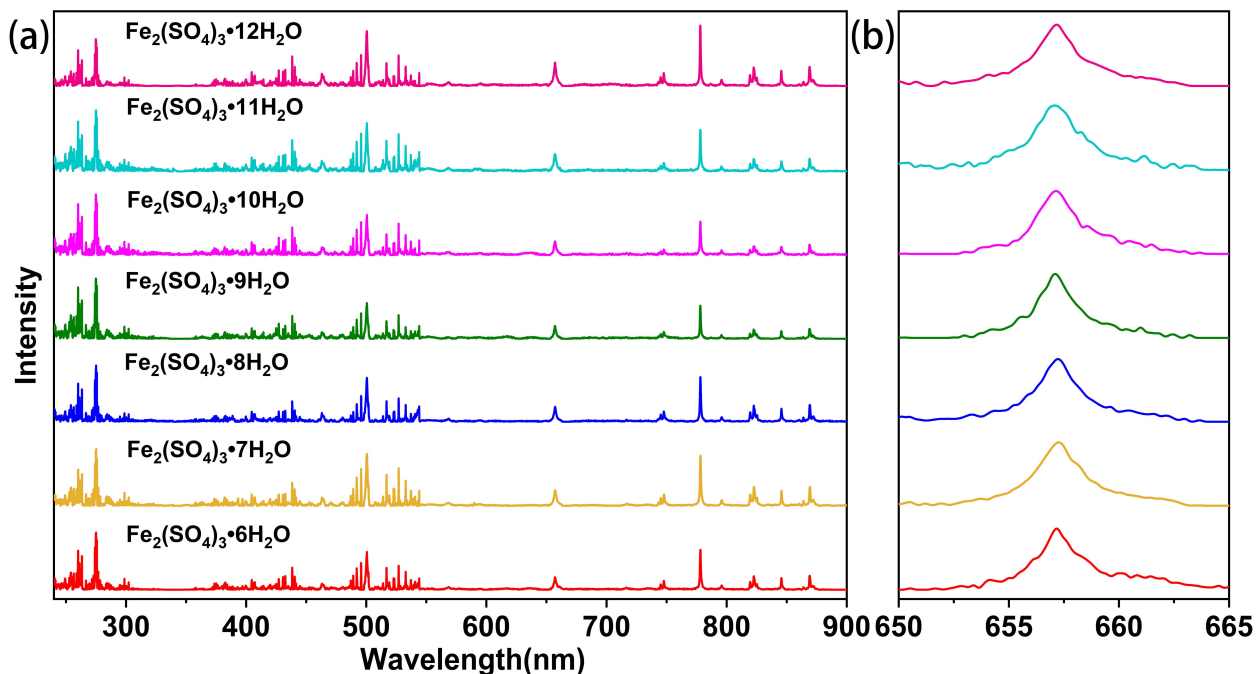

Figure 6. LIBS spectra of seven amorphous ferric sulfates. (a) the whole spectra from 238 to 900 nm of seven amorphous ferric sulfates; (b) the enlarged of Hα emission line at 656.7 nm.

3.5 The water content of synthesized ferric sulfates quantified by LIBS

A number of experimental parameters affect the standoff LIBS signal. They are related to laser irradiance (laser energy, focus, and distance to target), atmosphere (total pressure/density and composition), and target properties (different chemical/physical matrices and mixtures). However, those results do not affect quantifying the hydrogen content using the LIBS outputs. In order to eliminate the influence of accidental error, the obvious abnormal points were abandoned, and each sample was analyzed using five spectra. Subsequently, we normalize the signals in order to compensate as much as possible for the undesired effects of these parameters. The hydrogen content quantification was carried out through oxygen emission line intensity (778

340   nm) normalization for all twelve samples. The Gauss-Lorentz mixture function in WIRE 3.4
341   software was used to fit the H peak at 656.7 nm and the O peak at 778 nm, respectively.

342   For two system ferric sulfates samples, the value of the normalized peak intensity
343   increases monotonously as the number of H_2O molecules increases in the ferric sulfate
344   structures. In order to keep the H_2O molecules comparable among crystalline ferric sulfates, the
345   number of H_2O molecules of $Fe(OH)SO_4$ and $FeH(SO_4)_2 \cdot 4H_2O$ were calculated as one and nine,
346   respectively. Under Mars conditions, the linear regression equation for crystalline ferric sulfates
347   system is (Figure 7a):

348 $$A_{656.7/778} = 0.149W + 0.784, R^2 = 0.991$$

349   In Earth environment, the linear regression equation is (Figure 7b):

350 $$A_{656.7/778} = 0.0852W + 0.295, R^2 = 0.958$$

351   For amorphous ferric sulfates system, the linear regression equation is (Figure 7c):

352 $$A_{656.7/778} = 0.374W + 0.0467, R^2 = 0.955$$

353   where A is the area of LIBS emission line, $A_{656.7/778}$ is the area of Hα emission line at
354   656.7 nm normalized by O emission line at 778 nm, and W is the water content of the synthetic
355   ferric sulfates. These results demonstrated that the hydration states of the ferric sulfates can be
356   extracted from their LIBS spectra. This capability will be significant when encountering ferric
357   sulfates in a sampling spot on Mars and Earth.

358   Leave one out cross validation refers to extracting data points from a dataset one at a
359   time, fitting the remaining data, predicting the extracted data points with model results, and then
360   cycling until all data in the dataset have been extracted once. The use of RMSECV is common,
361   and it is considered an excellent general purpose error metric for numerical predictions (Thomas
362   et al., 2018). In order to evaluate the goodness of fit of the model, the root-mean-square error of
363   cross-validation (RMSECV) was calculated in this study, using the equation below:

$$RMSECV = \sqrt{\frac{\sum_{i=1}^{n}(y_i - \hat{y_i})^2}{n}}$$

364   In the formula, y_i is the true value measured by LIBS, $\hat{y_i}$ is the predicted value of cross-
365   validation, and n is the sum of all data points. The calculated RMSECV values of amorphous
366   ferric sulfates and crystalline ferric sulfates under Earth and Mars environment are 0.028, 0.130,
367   and 0.127, these results indicated that the fitting effect of our model is good, and also
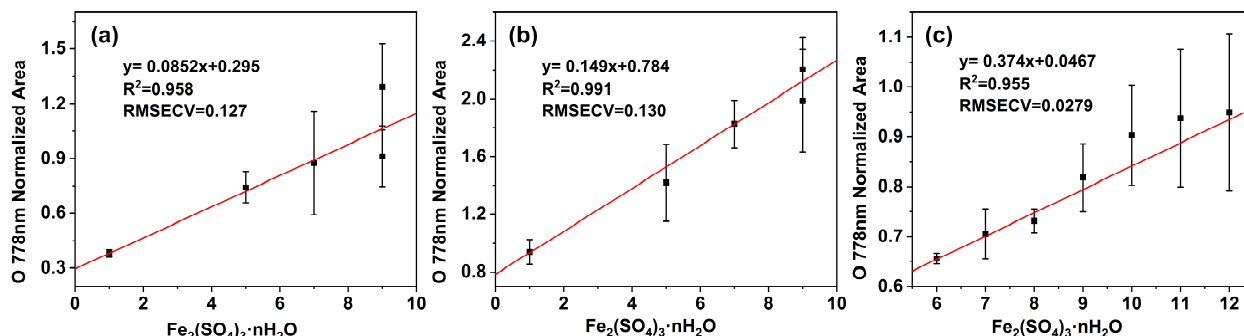368   demonstrated the feasibility of H quantification of different ferric sulfates by LIBS technique.

369

370

Figure 7. The linear fitting of the number of H_2O molecules in twelve ferric sulfates with O 778 nm normalized area. (a) is the five crystalline ferric sulfates measured under an Earth environment; (b) is the five crystalline ferric sulfates measured under Mars conditions; (c) is the seven amorphous ferric sulfates measured under an Earth environment. All of them showed a better linear relationship.

4 Discussion and implications

4.1 A new pathway of amorphous ferric sulfates occurred on Mars

The amorphous ferric sulfates were suggested widely on Mars, especially in the Gale Crater the amorphous ferric sulfates may be the candidate phase at some detected sites. In common, the volcanic activity, impacts, hydrothermal activity, and chemical weathering could lead to the amorphous phases formed in early Martain history (Shidare et al., 2021). The geological process of volcanic activity, impacts, and hydrothermal activity can be provided the source of heat and water to dissolve the igneous rock (e.g., Fe-olvine and sulfides). The chemical weathering at relative low temperature with acid fluids can also lead to the formation of amorphous phases. Except for these geological processes, the formation mechanisms of amorphous ferric sulfates were recognized by two main ways previously: (1) they formed by dehydration of saturated solution/fluids of ferric sulfates under lower relative humidity; and (2) as the high hydrated ferric sulfates dehydration products (Audouard et al., 2014; Sklute et al., 2015; Xu and Parise, 2012). In this study, the method to synthesize amorphous ferric sulfates by unsaturated ferric sulfate solution with different concentrations is different from the above two ways. This may provide a new mechanism to interpret the occurring amorphous ferric sulfates on Mars. In our experiment, lower-concentration ferric sulfate solutions tend to precipitate amorphous ferric sulfate with lower water content. The products of saturated solutions or fluids of $Fe_2(SO_4)_3$ tend to produce crystalline ferric sulfates (Sklute et al., 2015). Therefore, if the amorphous ferric sulfate on Mars is formed by the rapid evaporation of brine, it tends to be an unsaturated solution of large amounts of water.

In addition, the previous study showed that the number of H_2O molecules per $Fe_2(SO_4)_3$ maximum value is 11 (Wang et al., 2012). In the present study, the highest number of H_2O molecules in amorphous is 12 and the water budget of H_2O wt % is 35% indicating that the amorphous ferric sulfates were able to store more water without undergoing a phase transition and will contribute more to Mars' water cycle. For example, if these amorphous ferric sulfates were present on Mars at Gale Crater, they account for the percentage of the soil that will affect the water abundance determined by the results of Sample Analysis at Mars (SAM) and CheMin. It is calculated that amorphous ferric sulfate could account for ~ 6.8-9.4 wt % of the rockest soil

405   in the Gale Crater, assuming that the amorphous ferric sulfate water content is similar to
406   lausenite ($Fe_2(SO_4)_3 \cdot 6H_2O$) (Sklute et al., 2015).

407   4.2 Importance for phases identification of ferric sulfates on Mars

408   The crystalline ferric sulfates have also been proposed to exist on Mars at multiple
409   locations determined by VNIR and Mössbauer spectra. However, because of the similar spectra
410   features of hydrated crystalline ferric sulfates and other sulfates. The exact phases of the
411   crystalline ferric sulfates can not be constrained except jarosite. However, as shown in the
412   present study, the Raman spectra of five crystalline hydrated ferric sulfates have their unique
413   features indicating that the phases of hydrated ferric sulfates can be exactly identified by the
414   Raman spectroscopy. Moreover, the Raman spectroscopy can be used to distinguish between
415   crystalline ferric sulfates and amorphous ferric sulfates. For the different hydrated amorphous
416   ferric sulfates they can also be separated by their main SO_4 tetrahedron peak positions shifts
417   around 1000 cm^{-1}. The Mg-, Ca-, sulfates, and amorphous phases have been identified in Jezero
418   Crater soils and rocks by the Raman spectrometers, and the Fe- sulfates were determined at Cape
419   Nukshak, Yori Pass Outcrop in Jezero Crater by the Planetary Instrument for X-ray
420   Lithochemistry (PIXL) (Hurowitz et al., 2023; Lopez-Reyes et al., 2023; Phua et al., 2023).
421   However, the exact phases of Fe- and Mg- sulfates were not precisely constrained whether or not
422   they performed as crystalline or amorphous. If they are detected in the future by Raman
423   spectrometers, this study may provide a better reference to determine their phases, especially to
424   determine the hydration degree of amorphous ferric sulfates.

425   The elements information derived from their LIBS spectra can be used to assist in the
426   detection of different kinds of ferric sulfates at Gale Crater. The methods to quantify the major
427   elements have been matured by using multivariable analysis (David et al., 2020; Maurice et al.,
428   2016; Vogt et al., 2020). The ferric sulfates have been suggested to have occurred in Gale Crate
429   at different sites including the Rocknest soils, Naukluft Plateau and Vera Rubin Ridge by the
430   FeO_T weight percent as a function of weight percent of SO_3 or correlation with other elements
431   (David et al., 2020, 2022; L'Haridon et al., 2018). But the hydration states and the crystallinity of
432   these ferric sufates were not well constrained. The LIBS measurement results and the method of
433   water content quantification in this study can help to constrain the hydration states of ferric in
434   Gale Crater. For the Perseverance, if the LIBS employed on SuperCam combined with the
435   SHERLOC, not only the hydrated ferric sulfates but also all hydrated minerals hydration degrees
436   can be exactly determined in Jezero Crater.

437   4.3 Significance and applications of ferric sulfate water quantification

438   The Raman Spectrometer, which has been on board the Perseverance and will board
439   ExoMars in the future, can provide precise identification of the mineral phases and the
440   possibility of detecting organics on Mars. The hydrated minerals have been detected in Jezero
441   Crater, including the polyhydrated Mg-sulfates, Ca-sulfates, phyllosilicates, and amorphous
442   phases at Séítah and Máaz formations. This indicates aqueous alteration of the crater floor units.
443   However, the water content of these determined hydrated minerals and some of their exact
444   phases are not well constrained. This may be due to the fact that the methods are not available
445   and the definitive identification of hydration carriers can be complicated by coexisting materials,
446   and varying states of hydration. Those results will affect our understanding of the detailed
447   information of water and geochemical processes in the Jezero Crater. The relationship between

448 the water content and peak intensity, peak position, and peak area established in the present
449 study can be used as a better reference for the water quantification and the precise hydration state
450 detection of hydrated minerals determined in the Jezero Crater now and in Oxia Planum in the
451 future.

452   With the acquired data from the LIBS employed on the Curiosity, the hydrogen or water
453 content in soils and rocks was studied. As mentioned above, the main kinds of sulfates identified
454 in Gale Crater are Mg-, Fe-, and Ca- sulfates. The hydration states of calcium sulfates in veins
455 and magnesium sulfates in the Norwood Cove (crosses) and Beach Cliff (triangle) bedrock
456 fragments from the upper Murray formation heterolithic facies were derived by the hydrogen
457 weight percent versus the water content in different hydration states of calcium sulfates and
458 measurements of CaO and MgO weight percent (Nachon et al., 2014; Rapin et al., 2016, 2019).
459 It also means the methods were established to identify the Mg- and Ca- sulfates on Mars based
460 on LIBS technique. The ferric sulfates have no reliable method to determine on Mars by LIBS
461 even though there have been a lot of studies, such as Sobron et al.'s (2012) finding that the
462 relationship between hydrogen content and the H emission line area at 656 nm is irregular
463 (Sobron et al., 2012). In this study, the identification hydration degrees method for ferric sulfates
464 was developed by referring to the calcium sulfates and magnesium sulfates hydration degrees
465 determined methods based on LIBS from Rapin et al. in 2019 and 2016 (Rapin et al., 2016,
466 2019). As shown above, the number of H_2O molecules in ferric sulfate has a good relationship
467 with the O normalized area. These results can be used to help precisely constrain the phases of
468 ferric sulfates in Jezero Crater and Gale Crater.

469   4.4 Implications for water cycles on Mars

470   The hydrated minerals, such as clays, zeolites, and sulfates play a critical role in the water
471 cycle on current Mars. Even though Mars is arid and no liquids were observed on its surface, the
472 water cycle still exists between the atmosphere and the soils or minerals on Mars (Pommerol et
473 al., 2009). Two ways for the minerals or soils to keep the water. One is the H_2O molecules as
474 adsorbed on the mineral surface; another way is the H_2O stored in the crystalline structure. All
475 kinds of rocks and minerals can hold a certain amount of adsorbed water on their surface (Meslin
476 et al., 2013). When the temperature increases in the early daytime, the adsorbed water first goes
477 into the atmosphere. When the temperature reaches the maximum of the day, the structural water
478 in some minerals will released into the atmosphere. Compared with the amorphous phases, the
479 H_2O molecules in crystalline minerals release into the atmosphere is not easy. The amorphous
480 ferric sulfates are very sensitive to environmental parameter changes (Skulte et al., 2015). They
481 can not only hold a large amount of adsorbed water but also rehydrate and dehydrate very
482 quickly. The amorphous phases, especially amorphous ferric sulfates in soils and rocks may play
483 an important role in water diurnal cycles (Figure 8a). Compared with the amorphous sulfates, the
484 crystalline ferric sulfates tend to be more important in water seasonal cycles (Figure 8b), because
485 of the long duration of the phase change of crystalline ferric sulfates on the Martian surface. By
486 measuring the hydration states of different kinds of ferric sulfates or other hydrated minerals, we
487 can trace the climate evolution and the pathways of the water evolution at different times in one
488 Martain year between the atmosphere and the soils or minerals on current Mars.

489   In the Martian winter, the surface temperature is very low, probably below the release
490 temperature of water in the hydrated minerals of ferric sulfates (Wang et al., 2012, 2013). Water
491 molecules may exist mostly in the form of crystalline water in ferric sulfates, which is not easily

492   released into the atmosphere. When the spring and summer, the Martian surface's temperature
493   increases, the water molecules would be released from the ferric sulfates into the atmosphere to
494   form water vapor. As temperatures on the Martian surface begin to drop again, in the fall, the
495   ferric sulfates may absorb water molecules and store them in their crystalline structures (Figure
496   8b). Currently, most of the water is stored in polar ice caps or underground ice (Scheller et al.,
497   2021). With the temperature changes in different seasons, the ice and snow of the polar ice caps
498   will melt and release water molecules or the water vapor turns into water ice again in polar
499   regions (Figure 8b). These processes could affect the water status of hydrated minerals on the
500   Martian surface. In addition, the groundwater and Martian dust storms may also be involved in
501   the formation of ferric sulfates. The groundwater would participate in the weathering of minerals
502   in rocks to form hydrated minerals (Frydenvang et al., 2017; Michalski et al., 2013). The Martian
503   dust storms can increase the meridional circulation of the atmosphere, thereby enhancing water
504   vapor transport between the northern and southern hemispheres (Aoki et al., 2019, Figure 8b).
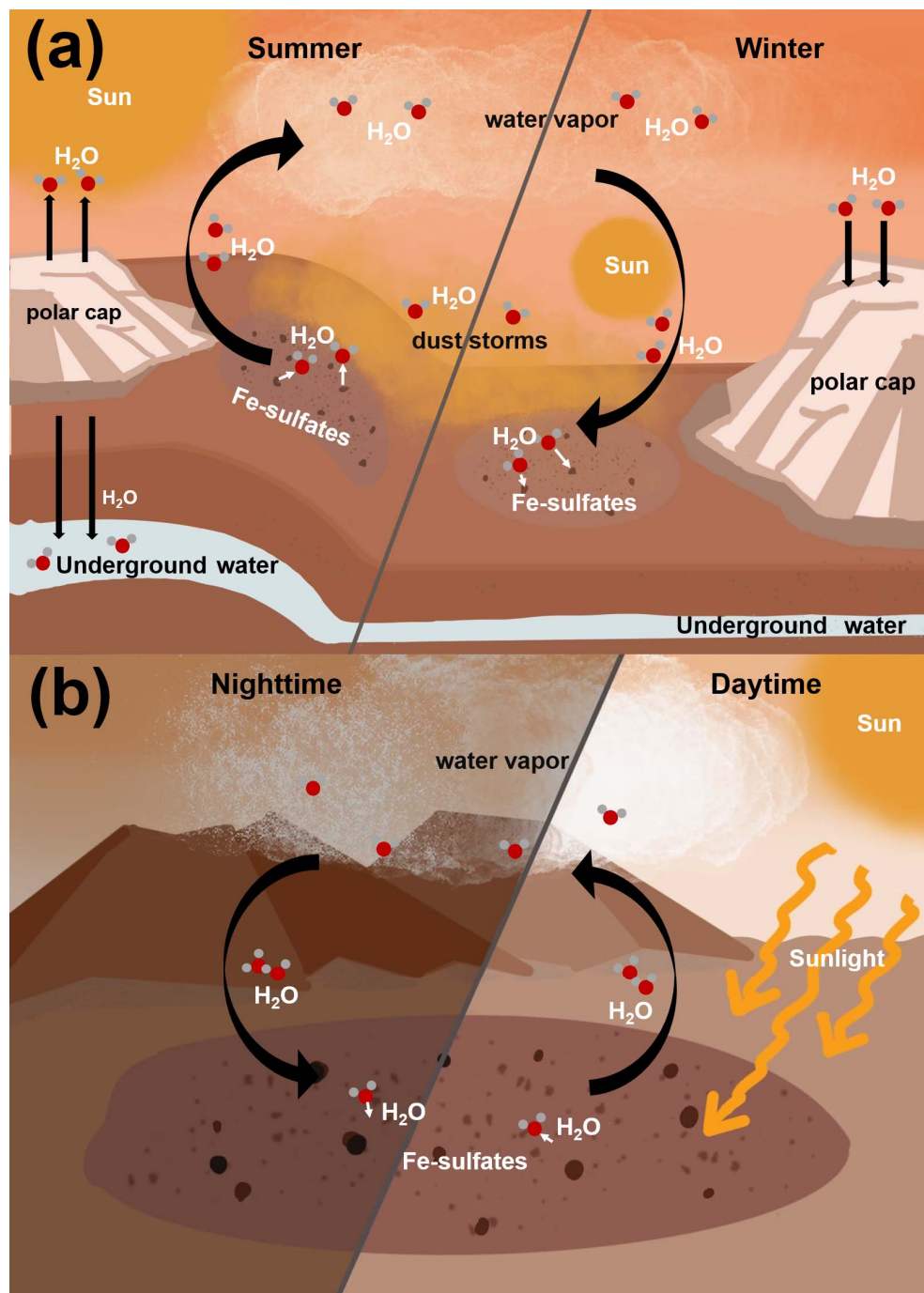
Figure 8. Schematic diagram of the Martian surface water cycle with ferric sulfates. (a) the role of ferric sulfates in water seasonal cycles on Mars surface; (b) the role of ferric sulfates in water diurnal cycles on Martian surface.

5 Conclusions

Twelve hydrated ferric sulfates were synthesized which contain five crystalline ferric sulfates and seven amorphous ferric sulfates. A new pathway was proposed to synthesize amorphous ferric sulfates from unsaturated solutions, which would help us understand the water cycle and geochemical processes on Mars. The number of H_2O in the structure for per $Fe_2(SO_4)_3$ from 6 to 12 in amorphous ferric sulfates. The relationship between its spectra features and water content was obtained. The linear relationship between the number of H_2O molecules in seven amorphous ferric sulfates and their Raman features (main SO_4 tetrahedron peak positions and the intensity and area ratios of SO_4 tetrahedron peak positions over water features) were established. Also, the linear relationship between the number of H_2O molecules and the $H\alpha$ emission line area at 656.7 nm normalized by O at 778 nm was developed. All of them have a good linear correlation with an R^2 value greater than 0.95. These results will provide a better reference for ChemCam, SuperCam, and the SHERLOC identified ferric sulfates on Mars, helping us to better understand the water cycle and aqueous history on Mars.

Author contributions

Fan Meng conducted seven amorphous ferric sulfates synthesis, characterization, and data analysis. Erbin Shi conducted five crystalline ferric sulfates synthesis, characterization, and data analysis. Fan Meng and Erbin Shi drafted the original manuscript. Changqing Liu helped in taking LIBS spectral measurements. Zongcheng Ling designed the research and provided laboratory, chemical reagent, instruments, and fund support and helped in ferric sulfates characterization, data analysis, and revision of the manuscript. All co-authors contributed to the discussions, interpretations, and writing.

Competing financial interests

The authors declare no competing financial interests.

Data Availability Statement

The digital file corresponding to the spectral data in the figures of this manuscript is available Meng et al. (2023), no user ID and password are required to access these data.

544 in drawing the Figures. This work is also supported by Physical-Chemical Materials Analytical

545 & Testing Center of Shandong University at Weihai.

546 **References**

547 Aoki, S., Vandaele, A. C., Daerden, F., Villanueva, G. L., Liuzzi, G., Thomas, I. R., et al. (2019).

548 Water Vapor Vertical Profiles on Mars in Dust Storms Observed by TGO/NOMAD. *Journal of*

549 *Geophysical Research: Planets, 124*(12), 3482–3497.

550 https://doi.org/https://doi.org/10.1029/2019JE006109

551 Audouard, J., Poulet, F., Vincendon, M., Milliken, R. E., Jouglet, D., Bibring, J.-P., et al. (2014).

552 Water in the Martian regolith from OMEGA/Mars Express. *Journal of Geophysical Research:*

553 *Planets, 119*(8), 1969–1989. https://doi.org/10.1002/2014JE004649

554 Bhartia, R., Beegle, L. W., DeFlores, L., Abbey, W., Razzell Hollis, J., Uckert, K., et al. (2021).

555 Perseverance's Scanning Habitable Environments with Raman and Luminescence for Organics

556 and Chemicals (SHERLOC) Investigation. *Space Science Reviews, 217*(4), 58.

557 https://doi.org/10.1007/s11214-021-00812-z

558 Bish, D. L., et al. (2013), X-Ray Diffraction Results from Mars Science Laboratory: *Mineralogy*

559 *of Rocknest at Gale Crater, Science, 341*(6153), 5, https://doi:10.1126/science.1238932.

560 Bishop, J. L., Yeşilbaş, M., Hinman, N. W., Burton, Z. F. M., Englert, P. A. J., Toner, J. D., et al.

561 (2021). Martian subsurface cryosalt expansion and collapse as trigger for landslides. *Science*

562 *Advances*, *7*(6), 1–14. https://doi.org/10.1126/sciadv.abe4459

563 Blake, D. F., Vaniman, D., Achilles, C., Anderson, R., Bish, D., Bristow, T., et al. (2012).

564 Characterization and Calibration of the CheMin Mineralogical Instrument on Mars Science

565 Laboratory. *Space Science Reviews, 170*(1), 341–399. https://doi.org/10.1007/s11214-012-9905-

566 1

567   Blake, D. F., Morris, R. V, Kocurek, G., Morrison, S. M., Downs, R. T., Bish, D., et al. (2013).

568   Curiosity at Gale Crater, Mars: Characterization and Analysis of the Rocknest Sand Shadow.

569   *Science, 341*(6153), 1239505. https://doi.org/10.1126/science.12395

570   Burns, R. G. (1987), Ferric Sulfates on Mars, *Journal of Geophysical Research-Solid Earth and*

571   *Planets, 92*(B4), E570-E574, https://doi:10.1029/JB092iB04p0E570.

572   Chevrier, V. F., & Altheide, T. S. (2008). Low temperature aqueous ferric sulfate solutions on

573   the surface of Mars. *Geophysical Research Letters*, *35*(22).

574   https://doi.org/https://doi.org/10.1029/2008GL035489

575   Chou, I.-M., Seal, R. R., & Wang, A. (2013). The stability of sulfate and hydrated sulfate

576   minerals near ambient conditions and their significance in environmental and planetary sciences.

577   *Journal of Asian Earth Sciences, 62*, 734–758.

578   https://doi.org/https://doi.org/10.1016/j.jseaes.2012.11.027

579   Cloutis, E. A., et al. (2006), Detection and Discrimination of Sulfate Minerals Using Reflectance

580   Spectroscopy, *Icarus, 184*(1), 121-157, https://doi:10.1016/j.icarus.2006.04.003.

581   David, G., Cousin, A., Forni, O., Meslin, P.-Y., Dehouck, E., Mangold, N., et al. (2020).

582   Analyses of High-Iron Sedimentary Bedrock and Diagenetic Features Observed With ChemCam

583   at Vera Rubin Ridge, Gale Crater, Mars: Calibration and Characterization. *Journal of*

584   *Geophysical Research: Planets, 125*(10), e2019JE006314.

585   https://doi.org/https://doi.org/10.1029/2019JE006314

586   David, G., Dehouck, E., Meslin, P.-Y., Rapin, W., Cousin, A., Forni, O., et al. (2022). Evidence

587   for Amorphous Sulfates as the Main Carrier of Soil Hydration in Gale Crater, Mars. *Geophysical*

588   *Research Letters, 49*(21), e2022GL098755.

589   https://doi.org/https://doi.org/10.1029/2022GL098755

590   Dyar, M. D., Breves, E., Jawin, E., Marchand, G., Nelms, M., O'Connor, V., et al. (2013).

591   Mössbauer parameters of iron in sulfate minerals. *American Mineralogist*, *98*(11–12), 1943–

592   1965. https://doi.org/10.2138/am.2013.4604

593   Feldman, W. C., Boynton, W. V, Tokar, R. L., Prettyman, T. H., Gasnault, O., Squyres, S. W., et

594   al. (2002). Global Distribution of Neutrons from Mars: Results from Mars Odyssey. *Science,*

595   *297*(5578), 75–78. https://doi.org/10.1126/science.1073541

596   Frydenvang, J., Gasda, P. J., Hurowitz, J. A., Grotzinger, J. P., Wiens, R. C., Newsom, H. E., et

597   al. (2017). Diagenetic silica enrichment and late-stage groundwater activity in Gale crater, Mars.

598   *Geophysical Research Letters, 44*(10), 4716–4724.

599   https://doi.org/https://doi.org/10.1002/2017GL073323

600   Glotch, T. D., Bandfield, J. L., Christensen, P. R., Calvin, W. M., McLennan, S. M., Clark, B.

601   C., et al. (2006). Mineralogy of the light-toned outcrop at Meridiani Planum as seen by the

602   Miniature Thermal Emission Spectrometer and implications for its formation. *Journal of*

603   *Geophysical Research: Planets, 111*(E12). https://doi.org/10.1029/2005JE002672

604   Golden, D. C., Ming, D. W., Morris, R. V, & Mertzman, S. A. (2005). Laboratory-simulated

605   acid-sulfate weathering of basaltic materials: Implications for formation of sulfates at Meridiani

606   Planum and Gusev crater, Mars. *Journal of Geophysical Research: Planets, 110*(E12).

607   https://doi.org/https://doi.org/10.1029/2005JE002451

608   Harmon, R. S., Russo, R. E., & Hark, R. R. (2013). Applications of laser-induced breakdown

609   spectroscopy for geochemical and environmental analysis: A comprehensive review.

610   *Spectrochimica Acta Part B: Atomic Spectroscopy, 87*, 11–26.

611   https://doi.org/10.1016/j.sab.2013.05.017

612   Hurowitz, J. A., Tice, M. M., Allwood, A. C., Cable, M. L., Bosak, T., Broz, A., et al. (2023).

613   The Petrogenetic History of the Jezero Crater Delta Front From Microscale Observations By the

614   Mars 2020 PIXL Instrument. Paper presented at 54th Lunar and Planetary Science Conference,

615   The Woodlands, Texas.

616   Jin, G. B., Wu, Z. C., Ling, Z. C., Liu, C.Q., Liu, W., Chen, W. X., & Zhang, L. (2022). A New

617   Spectral Transformation Approach and Quantitative Analysis for MarSCoDe Laser-Induced

618   Breakdown Spectroscopy (LIBS) Data. *Remote Sensing, 14*(16), 3960.

619   https://doi.org/10.3390/rs14163960

620   Johnson, J. R., J. F. Bell, E. Cloutis, M. Staid, W. H. Farrand, T. McCoy, M. Rice, A. Wang, &

621   A. Yen (2007), Mineralogic Constraints on Sulfur-Rich Soils from Pancam Spectra at Gusev

622   Crater, Mars, *Geophysical Research Letters, 34*(13), 6, https://doi:10.1029/2007gl029894.

623   King, P. L., & McLennan, S. M. (2010). Sulfur on Mars. *Elements, 6*(2), 107–112.

624   https://doi.org/10.2113/gselements.6.2.107

625   Lane, M. D., Bishop, J. L., Darby Dyar, M., King, P. L., Parente, M., & Hyde, B. C. (2008).

626   Mineralogy of the Paso Robles soils on Mars. *American Mineralogist, 93*(5–6), 728–739.

627   https://doi.org/10.2138/am.2008.2757

628   Lichtenberg, K. A., Arvidson, R. E., Morris, R. V, Murchie, S. L., Bishop, J. L., Fernandez

629   Remolar, D., et al. (2010). Stratigraphy of hydrated sulfates in the sedimentary deposits of Aram

630   Chaos, Mars. *Journal of Geophysical Research: Planets, 115*(E6).

631   https://doi.org/10.1029/2009JE003353

632   Ling, Z. C., & A. L. Wang (2010), A Systematic Spectroscopic Study of Eight Hydrous Ferric

633   Sulfates Relevant to Mars, *Icarus, 209*(2), 422-433, https://doi:10.1016/j.icarus.2010.05.009.

634   Liu, C. Q., Ling, Z. C., Wu, Z. C., Zhang, J., Chen, J., Fu, X. H., et al. (2022). Aqueous

635   alteration of the Vastitas Borealis Formation at the Tianwen-1 landing site. *Communications*

636   *Earth & Environment, 3*(1), 280. https://doi.org/10.1038/s43247-022-00614-3

637   Liu, C. Q., Z. C. Ling, J. Zhang, Z. C. Wu, H. C. Bai, & Y. H. Liu (2021), A Stand-Off Laser-

638   Induced Breakdown Spectroscopy (Libs) System Applicable for Martian Rocks Studies, *Remote*

639   *Sensing, 13*(23), 15, https://doi:10.3390/rs13234773.

640   Lopez-Reyes, G., Nachon, M., Veneranda, M., Beyssac, O., Madariaga, J. M., Manrique, J. A., et

641   al. (2023). *Anhydrite Detections by Raman Spectroscopy with Supercam at the Jezero Delta,*

642   *Mars*. Paper presented at 54th Lunar and Planetary Science Conference, The Woodlands, Texas.

643   L'Haridon, J., Mangold, N., Meslin, P.-Y., Johnson, J. R., Rapin, W., Forni, O., et al. (2018).

644   Chemical variability in mineralized veins observed by ChemCam on the lower slopes of Mount

645   Sharp in Gale crater, Mars. *Icarus, 311*, 69–86. https://doi.org/10.1016/j.icarus.2018.01.028

646   Madden, M. E. E., R. J. Bodnar, & J. D. Rimstidt (2004), Jarosite as an Indicator of Water-

647   Limited Chemical Weathering on Mars, *Nature, 431*(7010), 821-823,

648   https://doi:10.1038/nature02971.

649   Maurice, S., Clegg, S. M., Wiens, R. C., Gasnault, O., Rapin, W., Forni, O., et al. (2016).

650   ChemCam activities and discoveries during the nominal mission of the Mars Science Laboratory

651   in Gale crater, Mars. *Journal of Analytical Atomic Spectrometry, 31*(4), 863–889.

652   https://doi.org/10.1039/C5JA00417A

653   McEwen, A. S., L. Ojha, C. M. Dundas, S. S. Mattson, S. Byrne, J. J. Wray, S. C. Cull, S. L.

654   Murchie, N. Thomas, & V. C. Gulick (2011), Seasonal Flows on Warm Martian Slopes, *Science,*

655   *333*(6043), 740-743, https://doi:10.1126/science.1204816

656

657 Meng, F., Shi, E. B., Liu, C. Q., Ling, Z. C. (2023). Water Quantification of Amorphous and

658 Crystalline Ferric Sulfates Relevant to Mars-Laboratory Data.

659 http://dx.doi.org/10.6084/m9.figshare.24105564

660 Meslin, P.-Y., Gasnault, O., Forni, O., Schröder, S., Cousin, A., Berger, G., et al. (2013). Soil

661 Diversity and Hydration as Observed by ChemCam at Gale Crater, Mars. *Science, 341*(6153),

662 1238670. https://doi.org/10.1126/science.1238670

663 Michalski, J. R., Cuadros, J., Niles, P. B., Parnell, J., Deanne Rogers, A., & Wright, S. P. (2013).

664 Groundwater activity on Mars and implications for a deep biosphere. *Nature Geoscience, 6*(2),

665 133–138. https://doi.org/10.1038/ngeo1706

666 Moeller, R. C., Jandura, L., Rosette, K., Robinson, M., Samuels, J., Silverman, M., et al. (2021).

667 The Sampling and Caching Subsystem (SCS) for the scientific exploration of Jezero crater by the

668 Mars 2020 Perseverance rover. *Space Science Reviews, 217*, 1–43.

669 https://doi.org/10.1007/s11214-020-00783-7.

670 Morris, R. V, Ming, D. W., Blake, D. F., Vaniman, D. T., Bish, D. L., Chipera, S. J., et al.

671 (2013). *The Amorphous Component In Martian Basaltic Soil In Global Perspective From Msl*

672 *And Mer Missions*. Paper presented at 44th Lunar and Planetary Science Conference, The

673 Woodlands, Texas.

674 Nachon, M., Clegg, S. M., Mangold, N., Schröder, S., Kah, L. C., Dromart, G., et al. (2014).

675 Calcium sulfate veins characterized by ChemCam/Curiosity at Gale crater, Mars. *Journal of*

676 *Geophysical Research: Planets, 119*(9), 1991–2016. https://doi.org/10.1002/2013JE004588

677 Nakamoto, K. (1978), Infrared and Raman Spectra of Inorganic and Coordination Compounds,

678 Wiley, New York, 156(2), C47-C48.

679   Pathak, A. K., Kumar, R., Singh, V. K., Agrawal, R., Rai, S., & Rai, A. K. (2012). Assessment

680   of LIBS for spectrochemical analysis: a review. *Applied Spectroscopy Reviews, 47*(1), 14–40.

681   https://doi.org/10.1080/05704928.2011.622327

682   Perkins, J. J., Sharma, S. K., Clegg, S. M., Misra, A. K., Wiens, R. C., & Barefield, J. E. (2009).

683   *Remote Laser-induced Breakdown Spectroscopy (LIBS) Analysis of Hydrated Sulfates*. Paper

684   presented at 40th Lunar and Planetary Science Conference, The Woodlands, Texas.

685   Phua, Y., Ehlmann, B. L., Mandon, L., Siljeström, S., Razzell Hollis, J., & Bhartia, R. (2023).

686   *Characterizing Hydration in Alteration Minerals of Jezero Crater Geologic Units with*

687   *SHERLOC on Mars-2020*. Paper presented at 54th Lunar and Planetary Science Conference. The

688   Woodlands, Texas.

689   Pommerol, A., Schmitt, B., Beck, P., & Brissaud, O. (2009). Water sorption on martian regolith

690   analogs: Thermodynamics and near-infrared reflectance spectroscopy. *Icarus, 204*(1), 114–136.

691   https://doi.org/10.1016/j.icarus.2009.06.013

692   Rapin, W., Meslin, P. -Y., Maurice, S., Vaniman, D., Nachon, M., Mangold, N., et al. (2016).

693   Hydration state of calcium sulfates in Gale crater, Mars: Identification of bassanite veins. *Earth*

694   *and Planetary Science Letters, 452*, 197–205. https://doi.org/10.1016/j.epsl.2016.07.045

695   Rapin, W., Ehlmann, B. L., Dromart, G., Schieber, J., Thomas, N. H., Fischer, W. W., et al.

696   (2019). An interval of high salinity in ancient Gale crater lake on Mars. *Nature Geoscience,*

697   *12*(11), 889–895. https://doi.org/10.1038/s41561-019-0458-8

698   Scheller, E. L., Ehlmann, B. L., Hu, R., Adams, D. J., & Yung, Y. L. (2021). Long-term drying

699   of Mars by sequestration of ocean-scale volumes of water in the crust. *Science, 372*(6537), 56–

700   62. https://doi.org/10.1126/science.abc7717

701   Schröder, S., Meslin, P. -Y., Gasnault, O., Maurice, S., Cousin, A., Wiens, R. C., et al. (2015).

702   Hydrogen detection with ChemCam at Gale crater. *Icarus, 249*, 43–61.

703   https://doi.org/10.1016/j.icarus.2014.08.029

704   Shidare, M., Nakada, R., Usui, T., Tobita, M., Shimizu, K., Takahashi, Y., & Yokoyama, T.

705   (2021). Survey of impact glasses in shergottites searching for Martian sulfate using X-ray

706   absorption near-edge structure. *Geochimica et Cosmochimica Acta, 313*, 85–98.

707   https://doi.org/https://doi.org/10.1016/j.gca.2021.08.026

708   Sklute, E. C., H. B. Jensen, A. D. Rogers, & R. J. Reeder (2015), Morphological, Structural, and

709   Spectral Characteristics of Amorphous Iron Sulfates, *Journal of Geophysical Research: Planets,*

710   *120*(4), 809-830, https://doi:10.1002/2014je004784.

711   Sklute, E. C., A. D. Rogers, J. C. Gregerson, H. B. Jensen, R. J. Reeder, & M. D. Dyar (2018),

712   Amorphous Salts Formed from Rapid Dehydration of Multicomponent Chloride and Ferric

713   Sulfate Brines: Implications for Mars, *Icarus, 302*, 285-295,

714   https://doi:10.1016/j.icarus.2017.11.018.

715   Smith, R. J., McLennan, S. M., Sutter, B., Rampe, E. B., Dehouck, E., Siebach, K. L., et al.

716   (2022). X-Ray Amorphous Sulfur-Bearing Phases in Sedimentary Rocks of Gale Crater, Mars.

717   *Journal of Geophysical Research: Planets, 127*(5), 1–24. https://doi.org/10.1029/2021JE007128

718   Sobron, P., Wang, A., & Sobron, F. (2012). Extraction of compositional and hydration

719   information of sulfates from laser-induced plasma spectra recorded under Mars atmospheric

720   conditions — Implications for ChemCam investigations on Curiosity rover. *Spectrochimica Acta*

721   *Part B: Atomic Spectroscopy, 68*, 1–16. https://doi.org/10.1016/j.sab.2012.01.002

722   Thomas, N. H., Ehlmann, B. L., Anderson, D. E., Clegg, S. M., Forni, O., Schröder, S., et al.

723   (2018). Characterization of Hydrogen in Basaltic Materials With Laser-Induced Breakdown

724   Spectroscopy (LIBS) for Application to MSL ChemCam Data. *Journal of Geophysical*

725   *Research: Planets, 123*(8), 1996–2021. https://doi.org/10.1029/2017JE005467

726   Toulmin III, P., Clark, B. C., Baird, A. K., Keil, K., & Rose Jr, H. J. (1976). Preliminary results

727   from the Viking X-ray fluorescence experiment: The first sample from Chryse Planitia, Mars.

728   *Science, 194*(4260), 81–84. https://doi.org/10.1126/science.194.4260.81

729   Treiman, A. H., Bish, D. L., Vaniman, D. T., Chipera, S. J., Blake, D. F., Ming, D. W., et al.

730   (2016). Mineralogy, provenance, and diagenesis of a potassic basaltic sandstone on Mars:

731   CheMin X-ray diffraction of the Windjana sample (Kimberley area, Gale Crater). *Journal of*

732   *Geophysical Research: Planets, 121*(1), 75–106.

733   https://doi.org/https://doi.org/10.1002/2015JE004932

734   Vandenabeele, P., & Jehlička, J. (2014). Mobile Raman spectroscopy in astrobiology research.

735   *Philosophical Transactions of the Royal Society A: Mathematical, Physical and Engineering*

736   *Sciences, 372*(2030), 20140202. https://doi.org/10.1098/rsta.2014.0202

737   Vogt, D. S., Schröder, S., Rammelkamp, K., Hansen, P. B., Kubitza, S., & Hübers, H.-W.

738   (2020). CaCl and CaF emission in LIBS under simulated martian conditions. *Icarus, 335*,

739   113393. https://doi.org/10.1016/j.icarus.2019.113393

740   Wang, A. L., Korotev, R. L., Jolliff, B. L., & Ling, Z. C. (2015). Raman imaging of

741   extraterrestrial materials. *Planetary and Space Science, 112*, 23–34.

742   https://doi.org/10.1016/j.pss.2014.10.005

743   Wang, A. L., W. C. Feldman, M. T. Mellon, & M. P. Zheng (2013), The Preservation of

744   Subsurface Sulfates with Mid-to-High Degree of Hydration in Equatorial Regions on Mars,

745   *Icarus, 226*(1), 980-991, https://doi:10.1016/j.icarus.2013.07.020.

746 Wang, A. L., & Ling, Z. C. (2011), Ferric Sulfates on Mars: A Combined Mission Data Analysis

747 of Salty Soils at Gusev Crater and Laboratory Experimental Investigations, *Journal of*

748 *Geophysical Research: Planets, 116*, 22, https://doi:10.1029/2010je003665.

749 Wang, A. L., Ling, Z. C., J. J. Freeman, & W. G. Kong (2012), Stability Field and Phase

750 Transition Pathways of Hydrous Ferric Sulfates in the Temperature Range 50 Degrees C to 5

751 Degrees C: Implication for Martian Ferric Sulfates, *Icarus, 218*(1), 622-643,

752 https://doi:10.1016/j.icarus.2012.01.003.

753 Wang, A. L., & Y. H. Zhou (2014), Experimental Comparison of the Pathways and Rates of the

754 Dehydration of Al-, Fe-, Mg- and Ca-Sulfates under Mars Relevant Conditions, *Icarus, 234*, 162-

755 173, https://doi:10.1016/j.icarus.2014.02.003.

756 Wang, A. L., Y. C. Yan, D. M. Dyar, J. L. Houghton, W. M. Farrell, B. L. Jolliff, S. M.

757 McLennan, E. B. Shi, & H. K. Qu (2020), Amorphization of S, Cl-Salts Induced by Martian Dust

758 Activities, *Journal of Geophysical Research: Planets, 125*(12), 31,

759 https://doi:10.1029/2020je006701.

760 Wiens, R. C., Maurice, S., Barraclough, B., Saccoccio, M., Barkley, W. C., Bell, J. F., et al.

761 (2012). The ChemCam Instrument Suite on the Mars Science Laboratory (MSL) Rover: Body

762 Unit and Combined System Tests. *Space Science Reviews, 170*(1), 167–227.

763 https://doi.org/10.1007/s11214-012-9902-4

764 Wiens, R. C., Maurice, S., Robinson, S. H., Nelson, A. E., Cais, P., Bernardi, P., et al. (2021).

765 The SuperCam instrument suite on the NASA Mars 2020 rover: Body unit and combined system

766 tests. *Space Science Reviews, 217*, 1–87. https://doi.org/10.1007/s11214-020-00777-5

767   Wu, Z. C., Ling, Z. C., Zhang, J., Fu, X. H., Liu, C. Q., Xin, Y. Q., et al. (2021). A Mars

768   environment chamber coupled with multiple in situ spectral sensors for Mars exploration.

769   *Sensors, 21*(7), 2519. https://doi.org/10.3390/s21072519

770   Xu, W. Q., & Parise, J. B. (2012). Temperature and humidity effects on ferric sulfate stability

771   and phase transformation. *American Mineralogist, 97*(2–3), 378–383.

772   https://doi.org/10.2138/am.2012.3927

773   Xu, W. Q., N. J. Tosca, S. M. McLennan, & J. B. Parise (2009), Humidity-Induced Phase

774   Transitions of Ferric Sulfate Minerals Studied by in Situ and Ex Situ X-Ray Diffraction,

775   *American Mineralogist, 94*(11-12), 1629-1637, https://doi:10.2138/am.2009.3182